Hybrid cancellation of ripple disturbances arising in AC/DC converters

Andrea Bisoffi, Luca Zaccarian, Mauro da Lio, Carnevale Daniele

Hybrid cancellation of ripple disturbances arising in AC/DC converters

Andrea Bisoffi [c,1] Luca Zaccarian [b,c,2] Mauro Da Lio [c,1] Daniele Carnevale [d,3] and JET Contributors [a]

[a] *See the Appendix of F. Romanelli et al., Proc. of the 2014 IAEA Fusion Energy Conference, Saint Petersburg, Russia.*

[b] *CNRS, LAAS, 7 avenue du colonel Roche, F-31400 Toulouse, France and Univ. de Toulouse, LAAS, F-31400 Toulouse, France.*

[c] *Dipartimento di Ingegneria Industriale, University of Trento, Italy.*

[d] *Dipartimento di Ing. Civile e Ing. Informatica, University of Rome "Tor Vergata", Italy*

Abstract

In AC/DC converters, a peculiar periodic nonsmooth waveform arises, the so-called ripple. In this paper we propose a novel model that captures this nonsmoothness by means of a hybrid dynamical system performing state jumps at certain switching instants, and we illustrate its properties with reference to a three phase diode bridge rectifier. As the ripple corrupts an underlying desirable signal, we propound two observer schemes ensuring asymptotic estimation of the ripple, the first with and the second without knowledge of the switching instants. Our theoretical developments are well placed in the context of recent techniques for hybrid regulation and constitutes a contribution especially for our second observer, where the switching instants are estimated. Once asymptotic estimation of the ripple is achieved, the ripple can be conveniently canceled from the desirable signal, and thanks to the inherent robustness properties of the proposed hybrid formulation, the two observer schemes require only that the desirable signal is slowly time varying compared to the ripple. Exploiting this fact, we illustrate the effectiveness of our second hybrid observation law on experimental data collected from the Joint European Torus tokamak.

Key words: hybrid dynamical system, hybrid observer, power system, tokamak plasma, ripple

1 Introduction

Many engineering applications require power electronics in their actuators and often these power electronics are equipped with AC/DC converters whose switching nature produces a peculiar ripple disturbance. A similar disturbance on the torque arises in the presence of split ring commutators on the shaft of DC motors. Ripple disturbances may have damaging effects on control design, not only because they affect the actuation signal (like in a DC motor), but also because they often affect the power supply, thus possibly affecting all sensor measurements due to the magnetic coupling. This phenomenon is especially noticed in high-power applications such as tokamaks and plasma control [22]. One of the important features of the ripple is that its frequency is typically a known parameter with little uncertainty, because it is a multiple of the utility frequency in the electrical power grid, which is in turn tuned very finely to the values of either 50 or 60 Hz. Due to this fact, it appears natural to address the problem of ripple estimation and rejection using linear [8] or nonlinear [11, Ch. 8] regulation theory.

However, the peculiar non-smoothness of ripple disturbances makes them less prone to be addressed with classical continuous-time approaches and makes it an interesting problem to be tackled using hybrid regulation theory (see, e.g., the preliminary work in [13] and the more recent results in [3–5, 14] and references therein). These works, as well as the approach adopted here, are based

[1] Email: {andrea.bisoffi, mauro.dalio}@unitn.it.

[2] Work supported in part by the ANR project LimICoS contract number 12 BS03 005 01, by the iCODE institute, research project of the Idex Paris-Saclay, and by the University of Trento, grant OptHySYS. Email: zaccarian@laas.fr.

[3] Work supported by ENEA-EUROFUSION. This work has been carried out within the framework of the EUROfusion Consortium and has received funding from the Euratom research and training programme 2014-2018 under grant agreement No 633053. The views and opinions expressed herein do not necessarily reflect those of the European Commission. E-mail: daniele.carnevale@uniroma2.it

on the novel framework for the description of nonlinear hybrid dynamical systems in [9, 10]. In particular, the advantage of adopting that framework will be evident here because it enables us to exploit important robustness properties following from suitable regularity of the dynamics. We make large use of the robustness results established in [10, Chap. 7] to specifically address a "ripple cancellation" problem, wherein the ripple corresponds to a high-frequency perturbation affecting a slowly varying signal within an available measurement. Then the goal of our design is to estimate the ripple component that can be suitably subtracted from the measurement signal. To this end, we consider a general context where an unknown *constant* bias affects the measurement, we take care of this constant bias by incorporating a band-pass filter in our ripple observer, and then rely on the robustness results in [10, Cor. 7.27] to apply the scheme in the presence of slowly varying signals.

Our approach is much inspired by the recent results in [6] and the machinery given in [24, Thm. 2] (also reported in [7, Lemma 1] with a notation that resembles more closely the situation addressed here). We would also like to emphasize that a hybrid approach to tackle this problem does not seem to be the only viable one, because the ripple disturbance is indeed an absolutely continuous function and one may find ways to generate it with a nonsmooth continuous time approach (see, e.g., the results in [12] where a continuous-time exosystem is built that generates the absolute value of a cosine waveform). However, it remains unclear how to do this for the specific waveform characterized in here. Our results are also close in nature to those reported in [5, Sec. 4.2], where a hybrid exosystem also generates the absolute value of a cosine waveform. However, as compared to that result, we focus here on ripple signals that perform commutations at phases *different* from $\pm\pi/2$ (see also Remark 1). Alternative methods that are relevant in the proposed context pertain to the scientific area of observer design for switched systems, because one may think of the ripple as being generated by a suitable switching system. Then, one may follow the approaches in [20] if the active mode (or, equivalently, the jump times among modes) is known, or rely on the approaches of [1, 19, 21] and references therein, where the active mode is estimated online. In addition to requiring a reformulation of our model as a switched system (which seems to be possible due to the continuity of the ripple output), the problem with applying these switched observation laws is that it is unclear how to take into account the slowly varying signal affecting the output measurement. In our work we incorporate a band-pass filter to remove that component from our ripple observer, and then we use the robustness of our formulation to prove *rigorous* properties of our scheme under a reasonable timescale separation assumption. Conversely, within the active mode detection of the above works, this seems to be a nontrivial goal.

A preliminary version of this paper was presented in [2]. Here, as compared to [2], we give the proofs of our two main theorems, and we discuss the application of the proposed scheme to experimental signals from the Joint European Torus (JET) tokamak, whereas only simulation results were given in [2].

The paper is organized as follows: in Section 2 we introduce the hybrid model for the ripple generation and present the cancellation problem under consideration. In Sections 3 and 4 we illustrate the two proposed estimation schemes, and state and prove their desirable properties. Finally, in Section 5 we illustrate the effectiveness of the more general scheme on the experimental measurements from the JET tokamak. The notation used throughout the paper is that of [10]. An illustrative survey of this approach can be found in [9] and a brief review in [17, Sec. 2].

2 A hybrid model for the ripple-induced noise in measurement signals

Let us consider a simple physical example where a ripple disturbance arises, i.e., the three phase diode bridge rectifier depicted in Figure 1, where the valves are ideal diodes. This device converts a three-phase voltage to a mono-phase *almost* direct voltage, which is applied to a load, for example a resistor. The resulting voltage is *almost* direct because, due to the logic of conversion, a non smooth waveform, the ripple, is superposed to the ideal direct voltage.

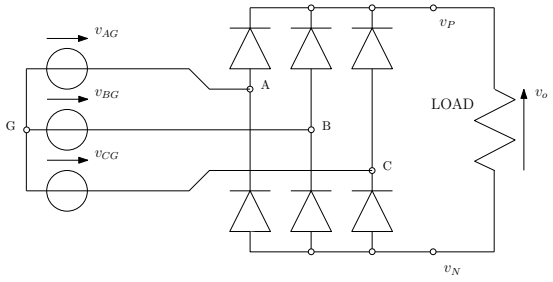

Figure 1. A three phase diode bridge rectifier for AC/DC conversion, which results in a waveform affected by a ripple.

Indeed, by denoting ground by G, the three phase voltages have the form:

$$\begin{aligned} v_{AG} &= v_A - v_G = V_f \sin(\omega t + \theta_0) \\ v_{BG} &= v_B - v_G = V_f \sin\left(\omega t + \theta_0 - \tfrac{2\pi}{3}\right) \\ v_{CG} &= v_C - v_G = V_f \sin\left(\omega t + \theta_0 - \tfrac{4\pi}{3}\right), \end{aligned} \tag{1}$$

and given the power supply in (1), the output voltage v_o of the converter in Figure 1 can be shown to be

$$v_o = v_P - v_N = \sqrt{3} V_f \max_{i\in\mathbb{Z}} \cos\left(\omega t + \theta_0 - i\tfrac{\pi}{3}\right). \tag{2}$$

This result follows easily from well-known circuit theory rules that establish the conducting diode, when more

than one are connected at cathode or anode. Over an interval $[0, T] = [0, 2\pi/\omega]$, (2) can be equivalently obtained by taking at each time the maximum among the three line-to-line voltages and their opposites in sign, as depicted in Figure 2.

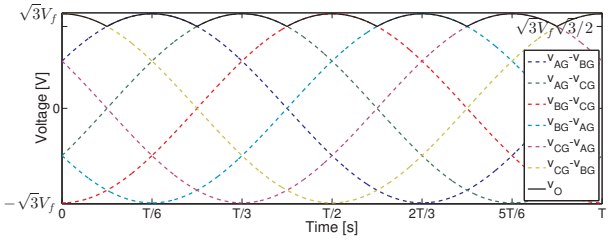

Figure 2. Line-to-line voltages in a three-phase diode bridge rectifier.

Based on the hybrid system formalism in [10], we propose a different characterization of the ripple and we show in Proposition 1 how it represents equivalently the physical example we have just introduced. The flow and jump dynamics read

$$\begin{cases} \dot{x}_r = \begin{bmatrix} 0 & -\omega \\ \omega & 0 \end{bmatrix} \begin{bmatrix} x_{r1} \\ x_{r2} \end{bmatrix} =: A_r x_r \\ \dot{\bar{b}} = 0 \end{cases}, \ (x_r, \bar{b}) \in \mathcal{C} \tag{3a}$$

$$\begin{cases} x_r^+ = \begin{bmatrix} 1 & 0 \\ 0 & -1 \end{bmatrix} \begin{bmatrix} x_{r1} \\ x_{r2} \end{bmatrix} =: J_r x_r \\ \bar{b}^+ = \bar{b} \end{cases}, \ (x_r, \bar{b}) \in \mathcal{D}, \tag{3b}$$

meaning that a solution can evolve according to the given differential or difference equation whenever the state belongs to $\mathcal{C}$ or to $\mathcal{D}$, respectively. The sets $\mathcal{C}$ and $\mathcal{D}$ are called intuitively flow and jump sets and are specified below. We use the following output equations:

$$y_r = x_{r1} + \bar{b} = \begin{bmatrix} 1 & 0 \end{bmatrix} x_r + \bar{b} =: C_r x_r + \bar{b} \tag{3c}$$

$$\theta = \angle(x_r). \tag{3d}$$

Output y_r in (3c) is the measured signal comprising a constant bias signal $\bar{b}$, whereas θ is *not* available for measurement (even though we may assume knowledge of its transition times, see Section 3). Function $\angle(\cdot)$ returns the phase of the vector at the argument, namely for each $x_r \neq 0$ it is the only angle $\theta \in [-\pi, \pi)$ satisfying $x_r = |x_r| \begin{bmatrix} \cos(\theta) \\ \sin(\theta) \end{bmatrix}$, which is well defined for all x_r satisfying $|x_r| \neq 0$. Note that function $\angle(\cdot)$ resembles the well known function atan2$(\cdot, \cdot)$ used in the robotics context.

The jump and flow sets in (3a)-(3b) are defined as

$$\mathcal{K} := \{(x_r, \bar{b}) \colon \delta \leq |x_r| \leq \Delta, |\bar{b}| \leq \Delta \text{ with } \Delta \geq \delta > 0\} \tag{3e}$$

$$\mathcal{C} := \{(x_r, \bar{b}) \colon -\pi/6 \leq \theta \leq \pi/6\} \cap \mathcal{K} \tag{3f}$$

$$\mathcal{D} := \{(x_r, \bar{b}) \colon \theta = \pi/6\} \cap \mathcal{K} \tag{3g}$$

and are depicted in Figure 3, where we added a possible solution to (3) flowing in $\mathcal{C}$ and jumping when it reaches $\mathcal{D}$. In $\mathcal{C}$ and $\mathcal{D}$, the intersection with the set $\mathcal{K}$ assumes that a nonzero ripple is actually present (δ strictly positive) but is bounded (existence of Δ). Indeed, $\delta \neq 0$ only excludes $|x_r| = 0$, corresponding to no ripple at all, and ensures that $\angle(\cdot)$ in (3d) is well defined. However, δ and Δ can be arbitrarily small and large, respectively, and *nowhere* in our design the knowledge of their values is required. Moreover, this choice enables us to deal with compact $\mathcal{C}$ and $\mathcal{D}$, so that (3) satisfies the so-called hybrid basic conditions [10, Assumption 6.5], and thus we can rely on useful results from [10, Chap. 7]. In particular, this allows us to derive our main result, Theorem 2, for the case of constant $\bar{b}$, but apply the corresponding scheme to the case of a slowly time varying signal $\bar{b}$ [10, Cor. 7.27].

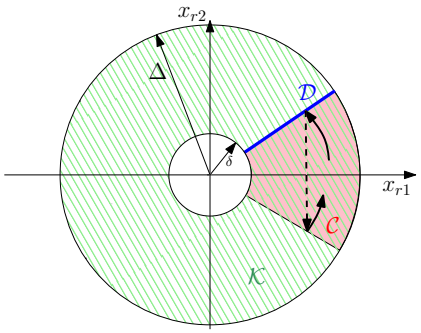

Figure 3. Sets $\mathcal{K}$, $\mathcal{C}$, $\mathcal{D}$ (projected on the plane (x_{r1}, x_{r2})) together with a possible trajectory (solid arrow for the flow and dashed arrow for a jump).

Remark 1 If the ripple was not generated by a three-phase system, we would consider a different angle in (3f) and (3g) instead of $\pi/6$. For example, for a 6-phase or a 12-phase system the angle would be respectively $\pi/12$ or $\pi/24$. ⌟

The following straightforward Proposition 1 motivates the study of ripple disturbances through the hybrid model (3). For its solutions we use hybrid time domains parametrized by two directions (t, j), where t denotes elapsed continuous time and j denotes elapsed discrete jumps (see [10, Chap. 2] and also [17, Sec. 2]). We constrain θ_0 to be in the set $[-\pi/6, \pi/6]$ because any other value of θ_0 could be shifted to this interval without changing the resulting value of v_o in (2). A relevant fact that we also establish below is that all solutions to (3) can be continued forward in time and have unbounded domain in the t direction of hybrid time (t, j) (this implies that all maximal solutions are complete [10, Sec. 2.3]).

Proposition 1 *For any value of* θ_0 *and* $V_f > 0$ *in (2), there exist initial conditions* $x_r(0,0) = \sqrt{3}V_f \begin{bmatrix} \cos\bar{\theta}_0 \\ \sin\bar{\theta}_0 \end{bmatrix}$

and $\bar{b}(0,0) = 0$ such that the unique solution to (3) has unbounded domain in the ordinary time direction and satisfies $y_r(t,j) = v_o(t)$, for all $(t,j) \in \mathrm{dom}(y_r)$.

Proof. First notice that (2) provides the same output for shifts of $\pi/3$ in θ_0 (due to the max). Therefore we consider without loss of generality $\theta_0 \in [-\pi/6, \pi/6]$ and $\bar{\theta}_0 = \theta_0$. We carry out the proof in polar coordinates that are globally defined in $\mathcal{C} \cup \mathcal{D}$. In particular, for a linear oscillator like (3a), the coordinate θ in (3d) evolves along flows according to $\dot{\theta} = \omega$. Moreover, by the definition of jump set (3g), as soon as $\theta = \pi/6$, (3b) in polar coordinates reads

$$\left(|x_r| \begin{bmatrix} \cos(\frac{\pi}{6}) \\ \sin(\frac{\pi}{6}) \end{bmatrix} \right)^+ = J_r |x_r| \begin{bmatrix} \cos(\frac{\pi}{6}) \\ \sin(\frac{\pi}{6}) \end{bmatrix} = |x_r| \begin{bmatrix} \cos(-\frac{\pi}{6}) \\ \sin(-\frac{\pi}{6}) \end{bmatrix},$$

showing that $|x_r|$ remains constant and θ changes sign across jumps. Therefore, each pair of consecutive jumps witnesses a dwell time of exactly $\pi/(3\omega)$ which is the time for θ to flow again from $-\pi/6$ to $\pi/6$. This shows dwell time of all solutions and proves that the domain of all solutions is unbounded in the ordinary time direction. Indeed, the flow and jump maps are Lipschitz single-valued functions and no flow is possible from the jump set, because the flow map $\dot{\theta} = \omega$ points out of $\mathcal{C} \cup \mathcal{D}$ (more rigorously, its intersection with the tangent cone to $\mathcal{C} \cup \mathcal{D}$ is empty – see [10, Prop. 6.10]). Therefore, the solution to (3) is unique. From (3a), $\frac{d}{dt}|x_r| = 0$ along flows and θ keeps revolving in the set $[-\pi/6, \pi/6]$, where $\cos(\theta)$ assumes its maximum. Therefore, all solutions starting from $\bar{b}(0,0) = 0$ satisfy

$$\begin{aligned} y_r(t,j) &= x_{r1}(t,j) = |x_r(t,j)| \cos(\theta(t,j)) \\ &= |x_r(0,0)| \max_{i \in \mathbb{Z}} \cos\left(\theta(0,0) + \omega t - i\tfrac{\pi}{3}\right), \end{aligned} \tag{4}$$

and then for $x_r(0,0) = \sqrt{3} V_f \left[\begin{smallmatrix} \cos\theta_0 \\ \sin\theta_0 \end{smallmatrix}\right]$ and $\theta(0,0) = \theta_0$ in (4), the (unique) solution to (3) satisfies the claim. □

Using Proposition 1, it is evident that in our motivating example we would like to track the zero-mean nonsmooth ripple disturbance

$$d(t) := v_o(t) - \frac{\omega}{2\pi} \int_0^{\frac{2\pi}{\omega}} v_o(\tau) d\tau = v_o(t) - \frac{3\sqrt{3} V_f}{\pi},$$

to get from $y_r(t)$ the direct voltage simply as $y_r(t) - d(t)$. Identity $\frac{\omega}{2\pi} \int_0^{\frac{2\pi}{\omega}} v_o(\tau) d\tau = \frac{6\omega}{2\pi} \int_{-\frac{2\pi}{12\omega} - \frac{\theta_0}{\omega}}^{\frac{2\pi}{12\omega} - \frac{\theta_0}{\omega}} \sqrt{3} V_f \cos(\omega\tau + \theta_0) d\tau = \frac{3\sqrt{3} V_f}{\pi}$ was used in the integral.

More generally, the goal of the paper can be formulated as follows.

Problem 1 *In a measurement y_r, a desirable signal σ is affected by a (nonsmooth, zero-mean) ripple disturbance d, i.e.,*

$$y_r = \sigma + d. \tag{5}$$

Our objective is to estimate asymptotically d only from y_r, so that we recover σ by trivial subtraction. We assume σ slowly varying compared to the timescale of d.

When the hybrid basic conditions are satisfied, [10, Cor. 7.27] establishes notably that if stability and convergence of an estimate $\hat{d}$ of d hold for a constant σ, then they are preserved also for a slowly varying σ thanks to inherent robustness properties, therefore in our design we will assume that σ be constant. Making explicit the setting of Problem 1 for model (3), we have

$$\begin{aligned} d(t,j) &:= y_r(t,j) - \bar{b}(t,j) - \tfrac{3}{\pi}|x_r(t,j)| \\ &= x_{r1}(t,j) - \tfrac{3}{\pi}|x_r(t,j)| && \text{(6a)} \\ \sigma(t,j) &:= \bar{b}(t,j) + \tfrac{3}{\pi}|x_r(t,j)| && \text{(6b)} \\ \hat{d}(t,j) &:= \hat{x}_{r1}(t,j) - \tfrac{3}{\pi}|\hat{x}_r(t,j)|, && \text{(6c)} \end{aligned}$$

which are respectively the zero-mean ripple disturbance, the (constant) desirable signal and the disturbance estimate.

3 Ripple estimation with knowledge of switching instants

If the switching instants of the ripple generator in (3) are known, it is possible to design an estimator consisting in a suitable Luenberger observer during flows and performing simultaneous jumps with the ripple generator (namely, the jump and flow sets remain unchanged and do *not* depend on the observer states). This corresponds to a simplified setting for the observer design. The assumption that the switching instants of the hybrid ripple generator are available to the ripple observer may be verified, for example, if the observation algorithm is connected to the circuitry commanding the switches of the rectifier in Figure 1, so that the switching times are known. Another case is that of a torque ripple generated by a DC motor where one may assume to measure the shaft angle and then compute the switching times based on the position of the split ring commutator.

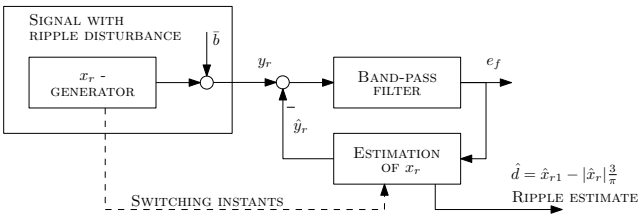

Figure 4. Scheme with generator, filter and hybrid observer of x_r when the switching instants are known.

The architecture of the proposed solution is sketched in Figure 4. The block "SIGNAL WITH RIPPLE DISTURBANCE" corresponds to hybrid system (3), whereas the block "BAND-PASS FILTER" corresponds to

$$F(s) := \frac{\frac{s}{\omega}}{\left(1+\frac{s}{\omega}\right)^2}, \tag{7}$$

with a double pole at the ripple frequency ω that isolates the dominant mode of the (nonsmooth) signal d from the constant bias and the high-frequency noise. The specific form of $F(s)$ is crucial to obtaining the structure below in (9) and the result of Lemma 1. The state-space representation of (7) is

$$\left[\begin{array}{c|c} A_f & B_f \\ \hline C_f & \end{array}\right] := \left[\begin{array}{cc|c} 0 & 1 & 0 \\ -\omega^2 & -2\omega & 1 \\ \hline 0 & \omega & \end{array}\right]. \tag{8a}$$

For the observer (block "ESTIMATION OF x_r") and filter dynamics, we add to (3) the following flow and jump equations

$$\begin{cases} \dot{x}_f = A_f x_f + B_f(y_r - \hat{y}_r) \\ \dot{\hat{x}}_r = A_r \hat{x}_r + L e_f, \end{cases} \qquad (x_r, \bar{b}) \in \mathcal{C} \tag{8b}$$

$$\begin{cases} x_f^+ = x_f \\ \hat{x}_r^+ = J_r \hat{x}_r, \end{cases} \qquad (x_r, \bar{b}) \in \mathcal{D}, \tag{8c}$$

and the following output equations

$$\begin{aligned} e_f &= C_f x_f \\ \hat{y}_r &= C_r \hat{x}_r \end{aligned} \tag{8d}$$

where $L := \left[\begin{smallmatrix} \ell \\ 0 \end{smallmatrix}\right]$ is the Luenberger gain and the scalar $\ell > 0$ is a design parameter. The flow and jump sets are the *same* as in (3) and depend *only* on output θ in (3d). We emphasize that to implement the hybrid observer (8) it is *not* necessary to measure θ, but only to know its switching times, that is, the times when the observer state $\hat{x}_r$ should jump.

To suitably analyze the overall system (3) and (8), let us introduce the error variable

$$e := \begin{bmatrix} \tilde{x}_r \\ \tilde{x}_f \end{bmatrix} := \begin{bmatrix} x_r - \hat{x}_r \\ x_f + A_f^{-1} B_f \bar{b} \end{bmatrix}, \tag{9a}$$

where $\tilde{x}_r$ is the error related to the ripple generation and $\tilde{x}_f$ is a coordinate transformation of the filter state variables chosen to satisfy $A_f \tilde{x}_f = A_f x_f + B_f \bar{b}$. Thanks to $\dot{\bar{b}} = 0$ and $C_f A_f^{-1} B_f = 0$, the (hybrid) error dynamics corresponds then to

$$\dot{e} = \begin{bmatrix} A_r & -LC_f \\ B_f C_r & A_f \end{bmatrix} e =: A_e e, \qquad (x_r, \bar{b}) \in \mathcal{C} \tag{9b}$$

$$e^+ = \begin{bmatrix} J_r & 0 \\ 0 & I_2 \end{bmatrix} e =: J_e e, \qquad (x_r, \bar{b}) \in \mathcal{D}, \tag{9c}$$

for which Lemma 1 holds.

Lemma 1 *Given dynamics* (3) *and* (8) *and the error dynamics (9), for every $\ell > 0$, the selection $L := \left[\begin{smallmatrix} \ell \\ 0 \end{smallmatrix}\right]$ in (8b) and (9b) ensures the existence of $P = P^T > 0$ and $H \in \mathbb{R}^{1\times 4}$ such that (H, A_e) is an observable pair and the function*

$$V(e) := e^T P e \tag{10}$$

satisfies

$$\langle \nabla V(e), A_e e \rangle = -e^T H^T H e, \qquad (x_r, \bar{b}) \in \mathcal{C} \tag{11a}$$

$$V(J_e e) - V(e) = 0, \qquad (x_r, \bar{b}) \in \mathcal{D}. \tag{11b}$$

Proof. Consider the diagonal $P := \left[\begin{smallmatrix} 1 & 0 & 0 & 0 \\ 0 & 1 & 0 & 0 \\ 0 & 0 & \omega^3\ell & 0 \\ 0 & 0 & 0 & \omega\ell \end{smallmatrix}\right]$. From $\ell > 0$, it follows $P = P^T > 0$. Moreover, using A_e in (9b), one obtains $PA_e + A_e^T P = \left[\begin{smallmatrix} 0 & 0 & 0 & 0 \\ 0 & 0 & 0 & 0 \\ 0 & 0 & 0 & 0 \\ 0 & 0 & 0 & -4\omega^2\ell \end{smallmatrix}\right] = -H^T H$, and $H := \left[\begin{smallmatrix} 0 & 0 & 0 & 2\omega\sqrt{\ell} \end{smallmatrix}\right]$. Then (11a) follows. As for H, the observability of the pair (H, A_e) is verified through the observability matrix $\left[\begin{smallmatrix} H^T & (HA_e)^T & (HA_e^2)^T & (HA_e^3)^T \end{smallmatrix}\right]^T$, whose determinant is $-16\omega^9\ell^2 \neq 0$. Finally,

$$\begin{aligned} V(e^+) - V(e) &= V(J_e e) - V(e) = e^T \left(J_e^T P J_e - P\right) e \\ &= e^T \left(\left[\begin{array}{c|cc} J_r^T J_r & \multicolumn{2}{c}{0} \\ \hline 0 & \omega^3\ell & 0 \\ & 0 & \omega\ell \end{array}\right] - P \right) e = 0 \end{aligned}$$

proves (11b), given that $J_r^T J_r = I_2$. □

Remark 2 The proof of Lemma 1 applies for any selection of the jump instants. Therefore the scheme in Figure 4 is effective at estimating the ripple y_r also when the jump set $\mathcal{D}$ is empty, which boils down to a standard linear disturbance rejection problem with an internal model. Due to this fact, our scheme can be seen as a generalization of the last one, much related to the recent works in [3–5, 14] and references therein. ⌟

Based on the Lyapunov construction of Lemma 1 we state next our first main result establishing asymptotic estimation of the ripple signal.

Theorem 1 *For every $\ell > 0$, the selection $L = \left[\begin{smallmatrix}\ell\\0\end{smallmatrix}\right]$ in (8b) and in (9b) guarantees that the compact attractor*

$$\mathcal{A} := \{(x_r, \bar{b}, \hat{x}_r, x_f) : \ e = 0 \text{ and } (x_r, \bar{b}) \in \mathcal{K}\}, \quad (12)$$

is uniformly globally exponentially stable for the closed-loop dynamics (3) *and* (8).

Proof. With Lyapunov function (10), the result is a direct consequence of [24, Thm. 2] (see also [7, Lemma 1] where a parallel formulation to this one is used). □

From (6a) and (6c) and (9a), the disturbance estimation error is

$$d - \hat{d} = \begin{bmatrix}1 & 0 & 0 & 0\end{bmatrix} e + \frac{3}{\pi}(|\hat{x}_r| - |x_r|),$$

so that Theorem 1 implies that for any positive choice of the scalar parameter ℓ, the estimate $\hat{d}$ converges uniformly and exponentially to the ripple disturbance d. Smaller selections of ℓ lead to slower convergence but are less sensitive to noise, whereas larger selections of ℓ lead to faster convergence but larger noise sensitivity should be expected.

4 Ripple estimation without knowledge of switching instants

In most practical cases it is difficult if not impossible to know the switching instants, and the scheme of the previous section cannot be implemented. This calls for the enhanced estimation scheme in Figure 5, where we estimate the switching instants by building an estimate $\hat{\theta}$ of the unavailable output θ in (3d).

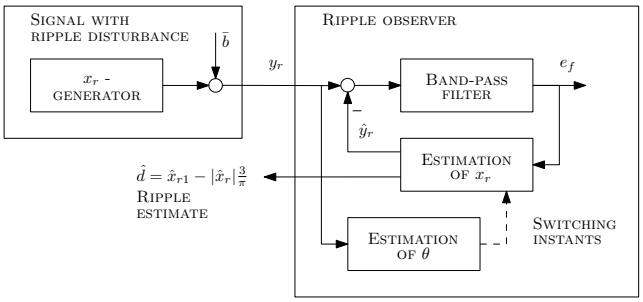

Figure 5. Scheme with generator, estimation of the switching instants, filter and hybrid observer of x_r when the switching instants are *not* known.

Remark 3 In the sequel, to keep the notation simple, we will introduce several coupled dynamical systems representing different components of the scheme in Figure 5 and having different jump and flow sets. These jump and flow sets will be specified in terms of only some state variables, implicitly meaning that the other state variables may assume any value within their respective domains. With this simplified notation we refer to the hybrid system constructed having flow set corresponding to the intersection of all the specified flow sets, flow map arising from stacking up all the specified flow equations (no flow equations will be repeated thus generating no ambiguity), jump set corresponding to the union of all the jump sets and jump map corresponding to the stack of all the specified jump maps. ⌟

Using the simplified notation mentioned in Remark 3, we preserve the main dynamics in (8) using a jump rule now triggered by the new state $\hat{\theta}$

$$\begin{cases} \dot{x}_f = A_f x_f + B_f(y_r - \hat{y}_r) \\ \dot{\hat{x}}_r = A_r \hat{x}_r + L e_f \\ \dot{\hat{\theta}} = \omega, \end{cases} \qquad \hat{\theta} \in \left[-\frac{\pi}{3}, \frac{\pi}{6}\right] \quad (13a)$$

$$\begin{cases} x_f^+ = x_f \\ \hat{x}_r^+ = J_r \hat{x}_r \\ \hat{\theta}^+ = \hat{\theta} - \pi/3, \end{cases} \qquad \hat{\theta} \in \left[\frac{\pi}{6}, \frac{\pi}{3}\right], \quad (13b)$$

with the same output equations (8d). Note that the lower bound on $\hat{\theta}$ in (13a) and the upper bound in (13b) are coarser than those in (8b) and (8c), because we want to leave some margin for suitable adaptation of $\hat{\theta}$.

Clearly, dynamics (13) converges to the right estimate when $\hat{\theta} = \theta$. The scheme is then completed by an additional action that updates periodically $\hat{\theta}$ in such a way that it converges to θ. Such convergence will be established based on the Lyapunov function:

$$V_\theta(\theta, \hat{\theta}) := \min_{i \in \mathbb{Z}} \left(\theta - \hat{\theta} + i\frac{\pi}{3}\right)^2 = \tilde{\theta}^2, \quad (14a)$$

$$\tilde{\theta} := \theta - \hat{\theta} + i^*\frac{\pi}{3}, \quad (14b)$$

$$i^* := \operatorname*{argmin}_{i \in \mathbb{Z}} \left(\theta - \hat{\theta} + i\frac{\pi}{3}\right)^2. \quad (14c)$$

In particular, the following lemma is fundamental to achieve this convergence property.

Lemma 2 *Consider any hybrid solution to solely* (3) *and* (13). *The output $\tilde{\theta}$ defined in (14b) and the Lyapunov function V_θ in (14a) both remain constant along flows and across jumps. Moreover, defining*[4] *for each $t \geq 0$*

[4] Note that the definition of $j^*(t)$ is valid for all $t \geq 0$ because all solutions have unbounded domain in the ordinary time direction, as established in Proposition 1.

the function $j^*(t) := \max_{(t,j)\in \mathrm{dom}\theta} j$, *the next identity holds:*

$$\int_t^{t+\frac{\pi}{3\omega}} \hat{\theta}\big(\tau, j^*(\tau)\big) d\big(\tau, j^*(\tau)\big) d\tau = -|x_r(0,0)|\rho(\tilde{\theta}), \tag{15}$$

where ρ *is such that* $\tilde{\theta} \mapsto \rho(\tilde{\theta})\tilde{\theta}$ *is a positive definite function in the interval* $\tilde{\theta} \in (-\pi/6, \pi/6)$ *and* d *is in* (6a), *corresponding to* $d = |x_r|\cos(\theta) - \frac{3}{\pi}|x_r|$.

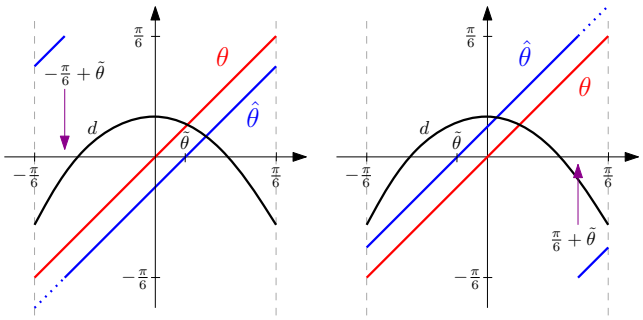

Figure 6. Proof for $\tilde{\theta} > 0$ (left) and $\tilde{\theta} < 0$ (right).

Proof. When one considers solely (3) and (13), $\tilde{\theta}$ and V_θ remain constant along solutions because $\dot{\theta} - \dot{\hat{\theta}} = \omega - \omega = 0$ along flows and $\theta^+ = \theta - \frac{\pi}{3}$ (similarly for $\hat{\theta}^+$) so that across jumps quantity i^* in (14c) changes but the minimum in (14a) does not.

Regarding integral (15), we compute it by dividing the analysis in the two cases shown in Figure 6. After some calculations, essentially splitting each integral in two parts, ρ in (15) can be found to be

$$\rho(\tilde{\theta}) := \begin{cases} -\frac{1}{6\omega}\Big(\pi - 6\tilde{\theta} - 2\pi\sin\big(\frac{\pi}{6} - \tilde{\theta}\big)\Big) =: \rho_p(\tilde{\theta}) & \tilde{\theta} \geq 0 \\ -\rho_p(-\tilde{\theta}) & \tilde{\theta} < 0 \end{cases}$$

so that $\tilde{\theta} \mapsto \rho(\tilde{\theta})\tilde{\theta}$ is positive definite in $(-\pi/6, \pi/6)$. □

Remark 4 As graphically illustrated in Figure 6, scalar $\tilde{\theta}$ characterized in Lemma 2 is the difference between θ and $\hat{\theta}$ modulo $\pi/3$, that is, by $\tilde{\theta}$ one measures their distance in a way that remains constant across jumps. ⌟

Based on the preliminary result of Lemma 2, we complete now the hybrid observer (13) with an additional dynamics implementing integral (15) and imposing suitable jump rules on $\hat{\theta}$ to ensure its convergence to θ. Consider

$$\begin{cases} \dot{\bar{y}}_r = 0 \\ \dot{\bar{y}}_{rI} = y_r - \bar{y}_r \\ \dot{\eta} = \hat{\theta}(y_r - \bar{y}_r) \\ \dot{\tau} = 1, \end{cases} \qquad \tau \leq \frac{\pi}{3\omega} \tag{16a}$$

$$\begin{cases} \bar{y}_r^+ = \bar{y}_r + k_{av}\dfrac{3\omega}{\pi}\bar{y}_{rI} \\ \bar{y}_{rI}^+ = 0 \\ \eta^+ = 0 \\ \tau^+ = 0 \\ \hat{\theta}^+ = \hat{\theta} - \mathrm{sat}_{\frac{\pi}{6}}(k_\theta \eta), \end{cases} \qquad \tau = \frac{\pi}{3\omega}, \tag{16b}$$

where $k_{av} \in (0, 1]$ and $k_\theta > 0$ are two positive gains to be tuned, and function $\mathrm{sat}_{\frac{\pi}{6}}(\cdot)$ is the scalar symmetric saturation function whose output is limited within $[-\pi/6, \pi/6]$. Note that this limitation ensures that $\hat{\theta}^+$ always belongs to the union of the flow and jump sets in (13), which guarantees existence of solutions. In (16), state τ is a periodic timer ensuring that integral (15) is computed periodically; over this period state $\bar{y}_{rI}$ integrates the difference between output y_r and its average value, so that $\bar{y}_r$ can converge to the average value of y_r. Finally, η implements left-hand side of (15) by subtracting the (estimated) average value $\bar{y}_r$ from measurement y_r and multiplying it by $\hat{\theta}$.

The overall ripple estimation scheme corresponds to the plant (3), the estimator dynamics in (13), and the extra flow and jump rules in (16), where the role of the different jump and flow sets should be intended as explained in Remark 3. The overall state is then given by

$$\xi := (x_r, \bar{b}, x_f, \hat{x}_r, \hat{\theta}, \bar{y}_r, \bar{y}_{rI}, \eta, \tau),$$

where we note that because $(x_r, \bar{b})$ belongs to the compact set $\mathcal{K}$ and $\tau \in [0, \pi/(3\omega)]$, then there exists a large enough scalar M such that $(\bar{y}_r, \bar{y}_{rI}, \eta, \tau) \in M\mathbb{B}^4$, where $\mathbb{B}^4$ is the four-dimensional closed unit ball. In the next theorem we establish parallel results to those of Theorem 1 in terms of stability properties of the attractor

$$\mathcal{A}_e := \mathcal{A} \times [-\pi/3, \pi/3] \times M\mathbb{B}^4, \tag{17}$$

where $\mathcal{A}$ is defined in (12) and corresponds to the set where the estimate $\hat{\theta}$ is correct. Note that Theorem 2 only establishes local properties of the scheme although its results could be *strengthened* by relying on a more sophisticated update law for $\hat{\theta}$ (see, e.g., [15] for global asymptotic stabilization of dynamics on bounded manifolds like our angles θ and $\hat{\theta}$) and on global results on cascaded hybrid systems.

Theorem 2 *For every* $\ell > 0$, *every* $k_{av} \in (0, 1]$ *and a small enough value of* $k_\theta > 0$, *the selection* $L := \left[\begin{smallmatrix} \ell \\ 0 \end{smallmatrix}\right]$ *in (13a) guarantees that the compact attractor* $\mathcal{A}_e$ *is uniformly locally asymptotically stable for the closed-loop dynamics (3), (13), (16).*

Proof. The scheme can be represented as the cascade of three hybrid dynamical systems.

The lowermost system corresponds to the dynamics restricted to the set

$$\mathcal{A}_\theta := \{\xi : \theta = \hat{\theta}\},$$

which is clearly forward invariant because the dynamics of $\hat{\theta}$ coincide with that of θ. Using the result of Theorem 1 it is readily seen that the dynamics restricted to $\mathcal{A}_\theta$ is UAS (actually UES) to $\mathcal{A}_e$.

The intermediate system corresponds to the dynamics restricted to the set

$$\mathcal{A}_{\bar{y}} := \{\xi : \bar{y}_r = \bar{b}(0,0) + \frac{3}{\pi}|x_r(0,0)|\}, \qquad (18)$$

which is again forward invariant because, from (6a) and (3), the scalar $\bar{b}(0,0) + \frac{3}{\pi}|x_r(0,0)|$ is the average value of $y_r(t, j^*(t))$, and $\bar{b}$ and $|x_r|$ remain constant along flows and across jumps. Also, the set $\mathcal{A}_\theta$ is uniformly (locally) asymptotically stable for the dynamics restricted to $\mathcal{A}_{\bar{y}}$. To establish this fact we use the Lyapunov function V_θ in (14a), which remains constant along flows (as established in Lemma 2). To analyze the change of V_θ across jumps, first note that in $\mathcal{A}_{\bar{y}}$ we have that $d = y_r - \bar{y}_r$. Then, due to periodicity of timer τ in (16) and due to the results of Lemma 2, we have before each jump in (16b) that $\eta = -|x_r(0,0)|\rho(\tilde{\theta})$. Therefore, across all such jumps, the quantity in (14b) satisfies

$$(\tilde{\theta}^+)^2 = \left(\theta - \hat{\theta}^+ + (i^*)^+\frac{\pi}{3}\right)^2 \leq \left(\theta - \hat{\theta}^+ + i^*\frac{\pi}{3}\right)^2 =$$
$$= \left(\tilde{\theta} - \mathrm{sat}_{\frac{\pi}{6}}\left(k_\theta|x_r(0,0)|\rho(\tilde{\theta})\right)\right)^2,$$

where the inequality follows from the fact that i^* in (14c) is a minimizer. Then from uniform boundedness of $|x_r(0,0)|$ and positive definiteness of $\tilde{\theta} \mapsto \rho(\tilde{\theta})\tilde{\theta}$ in the set $(-\pi/6, \pi/6)$, it is ensured that the function V_θ is (locally) strictly decreasing as long as $k_\theta > 0$ is sufficiently small. For all other jumps triggered by the jump sets in (3b) and (13b), function V_θ remains constant as established in Lemma 2. Since jumps in (16b) are periodic from periodicity of τ, then the asymptotic stability of $\mathcal{A}_\theta$ relative to initial conditions from $\mathcal{A}_{\bar{y}}$ follows from persistent jumping and [10, Prop. 3.24].

The uppermost system corresponds to the dynamics starting anywhere in the allowable set of initial conditions, which clearly converge to the attractor in (18). Indeed, at each jump triggered by (16b) it holds that $\frac{3\omega}{\pi}y_{rI}$ is the difference between the average of y_r, $\bar{b}(0,0) + \frac{3}{\pi}|x_r(0,0)|$, and its estimate $\bar{y}_r$, so that the update law in the first equation in (16b) leads to uniform convergence to zero of the Lyapunov function $V_y := (\bar{b} + \frac{3}{\pi}|x_r| - \bar{y}_r)^2$ (once again we apply [10, Prop. 3.24] and persistent jumping to establish this fact). Recall that $\bar{b}$ and $|x_r|$ remain constant along solutions, while $\bar{y}_r$ remains constant during flowing, so that V_y remains constant along flows and decreases across jumps thanks to $k_{av} \in (0, 1]$.

Once the three above nested (or cascade-like) results are established, the uniform (local) asymptotic stability of the innermost attractor given by $\mathcal{A}_e$ in (17) can be established applying iteratively the reasoning in [9, Corollary 19] by intersecting the flow and jump sets with sufficiently large compact sets. □

Remark 5 Small choices of k_{av} may be desired to suitably filter possible noise affecting the measurement. Similarly, k_θ should be selected small in such a way to ensure that Theorem 2 applies and that suitable noise rejection is obtained. In general, the tuning of the three parameters k_{av}, k_θ and ℓ should be carried out based on the cascaded structure of the proof. Indeed, to experience a graceful transient performance, it is reasonable to pick gain k_{av} as the most aggressive one, k_θ in such a way to induce an intermediate speed of convergence, and ℓ as the one that induces the slowest transient. This type of tuning procedure was adopted in Section 5. ⌟

5 JET experimental measurements

In this Section we apply the scheme in Figure 5 to experimental data collected from the JET tokamak [18]. For simulations confirming the effectiveness of the method presented in Section 4 in the case of *ideal nonsmooth* signals, we refer the reader to [2, Sec. V] while here we focus on the application of the scheme to experimental signals. The stabilization of the unstable plasma vertical position at JET facilities is achieved by changing the radial magnetic field produced by current flow on dedicated coils. Such a current is regulated by the Vertical Stabilization (VS) system by means of a current amplifier named ERFA. At the time of experiment ♯78000 (used here) a previous amplifier FRFA (Fast Radial Field Amplifier) was in place. The VS system acts on FRFA requesting a desired current $I_{\mathrm{FRFA,des}}$ that is obtained as the sum of two terms: the "fast" velocity loop that reacts promptly to plasma vertical displacements and the "slow" current loop that aims at regulating I_{FRFA} to zero. The ripple generated by the power electronics present in the experiment affects the feedback signal Z_{PD}, which is obtained by combining suitable magnetic measurements (from the Mirnov coils). For the current application we have

$$y_r(t) = \alpha\, I_{\mathrm{FRFA}}(t) + Z_{\mathrm{PD}}(t) \qquad (19)$$

where $I_{\mathrm{FRFA}}(t)$ is the current flowing within the poloidal coil and the scaling factor $\alpha = 4 \cdot 10^4$ m/s/A. All these quantities are depicted in Figure 7, where it is evident that the specific value of α in the linear combination (19) is selected to eliminate the current bursts around time 17.72 (to be found whenever a nonzero voltage is applied

to FRFA) and to let the ripple signal emerge in y_r. The resulting signal y_r is of clear graphical significance (the ripple effect was hidden in the oscillations within I_{FRFA} and Z_{PD}) but its experimental meaning is a subject of future work and goes beyond the goal of this paper. The experimental data on which we tested our hybrid observer are the useful 20-second portion of pulse ♯78000.

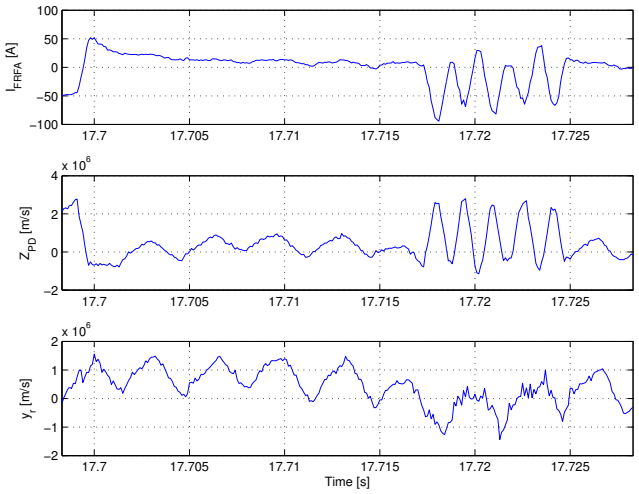

Figure 7. Experiment data from the JET tokamak: current I_{FRFA}, measurement Z_{PD} and their combination y_r.

To obtain a ripple-free signal, we apply the scheme in Figure 5 where we discard completely the "SIGNAL WITH RIPPLE DISTURBANCE" block and we inject directly into the "RIPPLE OBSERVER" block the signal y_r in (19). As a matter of fact, we have no longer a constant signal on which the ripple disturbance is superposed, but a signal that varies slowly with respect to the frequency of the ripple, as one can see from the bottom of Figure 7. As clarified after Problem 1, our solution also applies to this case, as long as the signal $\bar{b}$ is sufficiently slowly varying. In particular, the following Corollary of Theorem 2 follows from [10, Corollary 7.27], the fact that $\mathcal{A}_e$ in (17) is compact, and that dynamics (3), (13), (16) satisfy the hybrid basic conditions of [10, Assumption 6.5].

Corollary 1 *For every $\ell > 0$, every $k_{av} \in (0, 1]$ and a small enough value of $k_\theta > 0$, the selection $L := \left[\begin{smallmatrix}\ell\\0\end{smallmatrix}\right]$ in (13a) guarantees that the compact attractor $\mathcal{A}_e$ in (17) is uniformly locally asymptotically stable for the closed-loop dynamics (3), (13), (16), with the second equation in (3a) replaced by $\dot{\bar{b}} \in [-\rho_b, \rho_b]$, where ρ_b is a sufficiently small positive constant.*

Note that the modified dynamics for $\bar{b}$ in the above statement enables considering "biases" that are varying at sufficiently small rate ρ_b. According to the discussion after Problem 1 (see Eqs. (5) and (6c)) the signal resulting from the ripple cancellation filter corresponds to

$$\hat{\sigma} := y_r - \hat{d} = y_r - \big(\hat{x}_{r1} - \frac{3}{\pi}|\hat{x}_r|\big). \tag{20}$$

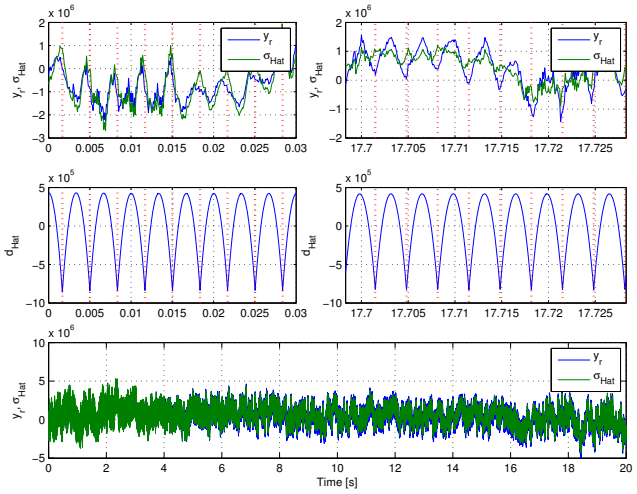

Figure 8. Original signal y_r, desirable signal $\hat{\sigma}$ and ripple estimate $\hat{d}$ in different timescales.

Figure 8 is obtained for the following parameters and initial values of the hybrid observer in (13) and (16): $\ell = 7.5$, $k_{av} = 0.9$, $k_\theta = 1$, $\bar{y}_r(0,0) = -0.5 \cdot 10^6$, $\bar{y}_{rI}(0,0) = 0$, $\eta(0,0) = 0$, $\tau(0,0) = 0$, $\hat{\theta}(0,0) = 0$, $x_f(0,0) = \left[\begin{smallmatrix}0\\0\end{smallmatrix}\right]$, $\hat{x}_r(0,0) = \left[\begin{smallmatrix}9.6\cdot 10^6\\0\end{smallmatrix}\right]$ (leading to a phase shift of roughly 90°). Following the discussion in [2, Sec. V-A] about implementing slightly inflated versions of flow and jump sets, in the current case of JET measurements we used only $\{\xi\colon \frac{\pi}{3\omega} \le \tau \le 1.005\frac{\pi}{3\omega}\}$ instead of $\{\xi\colon \tau = \frac{\pi}{3\omega}\}$ since we have no longer a ripple generator. This forces the maximal hybrid solutions to be also complete [10, Chap. 2.2 and 2.3] and prevents numerical perturbations from bringing solutions out of $\mathcal{C} \cup \mathcal{D}$, leading to premature termination of complete solutions. At the bottom of Figure 8 we have both y_r and $\hat{\sigma}$ on the full timescale. In the upper part, the beginning of the time history is zoomed on the left, and the end on the right (same zoom as in Figure 7). The red vertical lines correspond to the instants when the *estimate* $\hat{\theta}$ jumps: at the beginning they are not in phase with the original signal y_r while at the end they are, so that after convergence the hybrid observer effectively removes from y_r the ripple disturbance $\hat{d}$ in the right central part of Figure 8.

We compare our hybrid approach with one based on the internal model (IM) principle for linear systems [8]. According to the latter, we may approximate the ripple disturbance d in y_r by a *pure* sinusoid with frequency 6ω, deliberately neglecting its nonsmoothness and thereby accepting a steady-state residual error. Then a standard unity-feedback system as in Figure 10 guarantees that $\hat{d}^{IM}$ approximately manages to converge to the main linear harmonic in d, and by subtracting $\hat{d}^{IM}$ from y_r one gets asymptotically some linear estimate $\hat{\sigma}^{IM}$ of the desirable signal σ. We note that the coefficients κ_1 and κ_2 in $IM(s)$ affect mainly the transient, and are less relevant for the (approximately) asymptotic tracking we

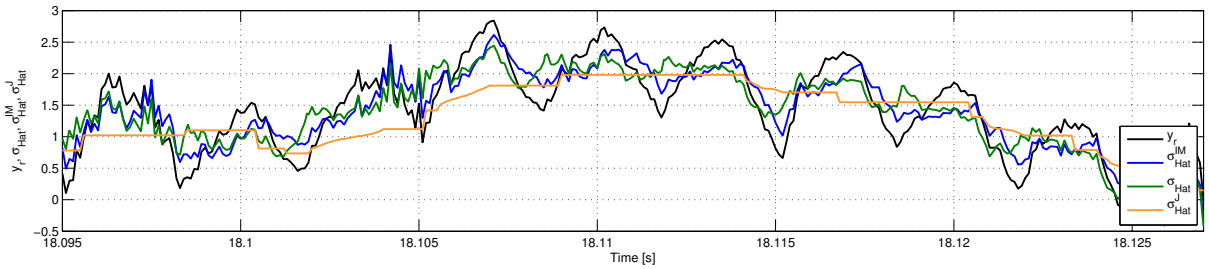

Figure 9. Original signal y_r and signals deprived of ripple: $\hat{\sigma}$ with our approach, $\hat{\sigma}^{IM}$ with internal model scheme, $\hat{\sigma}^{J}$ by solving an estimation problem.

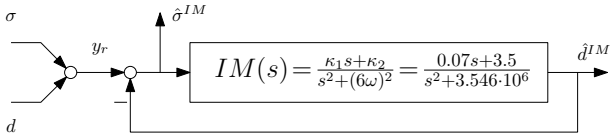

Figure 10. Internal model scheme and signals.

want to show in Figure 9. The resulting $\hat{\sigma}^{IM}$ from this approach is plotted in Figure 9 together with $\hat{\sigma}$ from our hybrid approach, which provides an improved estimation because it is based on a more accurate model of the specific ripple waveform. In particular, note that the linear cancellation scheme exhibits noticeable errors where the ripple waveform is not differentiable.

We also compare our approach with the solution of a (nonlinear) optimization problem exploiting numerical tools. Consider as cost function the squared error between the (sampled) output y_r and the estimated signal $\hat{y}_r$ over a window of N past samples, that is,

$$J_N(k) := \sum_{i=0}^{N-1} \left(y_r(t_{k-i}) - \hat{y}_r(t_{k-i})\right)^2 \tag{21}$$

$$\hat{y}_r(t_j) = \hat{\sigma}_j^J + \sqrt{3}V_f \max_{i\in\mathbb{Z}} \cos\left(\omega t_j + \theta_j - i\frac{\pi}{3}\right) - \frac{3\sqrt{3}}{\pi}V_f,$$

The minimization variables (in $\hat{y}_r$) are θ_k and $\hat{\sigma}_k^J$, and their optimal values are found iterating a numerical gradient descent algorithm on J_N (`fmincon()` of the optimization toolbox of Matlab®). In our case we have $V_f = 1.8 \cdot 10^6$ and we take $N = 30$ samples, and the result is shown in Figure 9. This approach is similar to the one proposed in [16, 23] where Newton and extremum-seeking techniques have been exploited to minimize J_N. With this approach the computational complexity is much higher, the time spent by iterations at each new sample to provide the new value of θ_k and $\hat{\sigma}_k^J$ is not known a priori, and the resulting $\hat{\sigma}_k^J$ can be nonsmooth. Important high frequency information could be canceled out by this approach, whose proof of convergence is in general a difficult problem and has not been addressed for the considered example.

Although our hybrid observer scheme is presented for offline experimental data, we finally emphasize that it can be used for estimating and removing the ripple *on line*, so that an estimate of the desirable signal $\hat{\sigma}$ in (20) is available for feedback purposes.

6 Conclusions

We proposed a hybrid dynamical system to model the ripple phenomenon arising in the context of power electronics. In particular, we discussed its effectiveness illustrating its (hybrid) solutions, flow/jump dynamics and sets with a three phase diode bridge rectifier. We proposed two hybrid schemes capable of asymptotically estimating the state of the hybrid model that generates the ripple waveform both when the switching instants are known and unknown. The proposed methodology was applied to reconstruct the ripple disturbance affecting experimental data of the vertical stabilization system at the JET facilities.

Acknowledgements. The authors would like to thank Fulvio Forni for useful discussions.

References

[1] J.P. Barbot, H. Saadaoui, M. Djemai, and N. Manamanni. Nonlinear observer for autonomous switching systems with jumps. *Nonlinear Analysis: Hybrid Systems*, 1(4):537–547, 2007.

[2] A. Bisoffi, M. Da Lio, and L. Zaccarian. A hybrid ripple model and two hybrid observers for its estimation. In *IEEE 53rd Conference on Decision and Control*, Los Angeles (CA), USA, 2014.

[3] D. Carnevale, S. Galeani, and L. Menini. Output regulation for a class of linear hybrid systems. Parts 1 & 2. In *IEEE 51st Conference on Decision and Control*, 2012.

[4] D. Carnevale, S. Galeani, and M. Sassano. Necessary and sufficient conditions for output regulation in a class of hybrid linear systems. In *IEEE 52nd Conference on Decision and Control*, pages 2659–2664, 2013.

[5] N. Cox, L. Marconi, and A. R. Teel. High-gain observers and linear output regulation for hybrid exosystems. *International Journal of Robust and Nonlinear Control*, 2013.

[6] F. Forni, A. R. Teel, and L. Zaccarian. Follow the bouncing ball: global results on tracking and state estimation

with impacts. *IEEE Transactions on Automatic Control*, 58(6):1470–1485, 2013.

[7] F. Forni, A. R. Teel, and L. Zaccarian. Reference mirroring for control with impacts. In J. Daafouz, S. Tarbouriech, and M. Sigalotti, editors, *Hybrid Systems with Constraints*, pages 211–249. Wiley, 2013.

[8] B. A. Francis and W. M. Wonham. The internal model principle of control theory. *Automatica*, 12(5):457–465, 1976.

[9] R. Goebel, R. Sanfelice, and A. R. Teel. Hybrid dynamical systems. *IEEE Control Systems Magazine*, 29(2):28–93, 2009.

[10] R. Goebel, R. G. Sanfelice, and A. R. Teel. *Hybrid Dynamical Systems: modeling, stability, and robustness*. Princeton University Press, 2012.

[11] A. Isidori. *Nonlinear Control Systems*. Springer, 3rd edition, 1995.

[12] L. Marconi and L. Praly. Uniform practical nonlinear output regulation. *IEEE Transactions on Automatic Control*, 53(5):1184–1202, 2008.

[13] L. Marconi and A. R. Teel. A note about hybrid linear regulation. In *IEEE 49th Conference on Decision and Control*, pages 1540–1545, 2010.

[14] L. Marconi and A. R. Teel. Internal model principle for linear systems with periodic state jumps. *IEEE Transactions on Automatic Control*, 58(11):2788–2802, 2013.

[15] C. G. Mayhew, R. G. Sanfelice, and A. R. Teel. Quaternion-based hybrid control for robust global attitude tracking. *IEEE Transactions on Automatic Control*, 56(11):2555–2566, 2011.

[16] P. E. Moraal and J. W. Grizzle. Observer design for nonlinear systems with discrete-time measurements. *IEEE Transactions on Automatic Control*, 40(3):395–404, 1995.

[17] D. Nešić, A. R. Teel, and L. Zaccarian. Stability and performance of SISO control systems with first-order reset elements. *IEEE Transactions on Automatic Control*, 56(11):2567–2582, 2011.

[18] A. Neto, G. De Tommasi, R. Albanese, G. Ambrosino, M. Ariola, G. Artaserse, A. J. N. Batista, B. Carvalho, F. Crisanti, H. Fernandes, et al. Exploitation of modularity in the JET tokamak vertical stabilization system. *Control Engineering Practice*, 20(9):846–856, 2012.

[19] S. Petterson. Switched state jump observers for switched systems. In *Proceedings of the 16th IFAC World Congress, Prague, Czech Republic*, 2005.

[20] S. Pettersson. Observer design for switched systems using multiple quadratic Lyapunov functions. In *Intelligent Control, 2005. Proceedings of the 2005 IEEE International Symposium on, Mediterrean Conference on Control and Automation*, pages 262–267. IEEE, 2005.

[21] S. Pettersson. Designing switched observers for switched systems using multiple Lyapunov functions and dwell-time switching. In *2nd IFAC Conference on Analysis and Design of Hybrid Systems*, volume 2, pages 18–23, 2006.

[22] A. Pironti and M. Walker. Fusion, tokamaks, and plasma control: an introduction and tutorial. *IEEE Control Systems Magazine*, 25(5):30–43, 2005.

[23] M. Sassano, D. Carnevale, and A. Astolfi. Extremum seeking-like observer for nonlinear systems. *IFAC Proceedings Volumes*, 44(1):1849 – 1854, 2011. 18th IFAC World Congress.

[24] A. R. Teel, F. Forni, and L. Zaccarian. Lyapunov-based sufficient conditions for exponential stability in hybrid systems. *IEEE Transactions on Automatic Control*, 58(6):1591–1596, 2013.